

A CFD Study to Understand the Role of Surface Textures on Erosive Wear

*Adil Keku Gazder
Department of Mechanical Engineering
Shiv Nadar University
December 2021*

The content, materials, and any other elements associated with this project, including but not limited to text, graphics, images, code, and design, are the intellectual property of the author and are protected by copyright law. Any commercial use or distribution of the materials without prior written consent from the author is strictly prohibited.

iii. Acknowledgements

Though the pandemic brought on several difficulties along the way, our research work was able to proceed uninterrupted thanks to the constant support and guidance of Dr. Harpreet Singh Grewal at every step of the way. I would not have learnt as much as I did without sir's mentorship and counsel. My parents and friends have always been there to support me and for that I am grateful. I would also like to express my gratitude towards Amit Sharma, Mayank Garg, Arunesh Kumar and Gopinath Perumal who have supported me extensively during the course of my work. Lastly, I would like to thank the Department of Mechanical Engineering, Shiv Nadar University for this opportunity to contribute to this field by which I am constantly fascinated.

Table Of Contents

S. No.	Content	Page No.
i.	Candidate Declaration	1
ii.	Certificate	2
iii.	Acknowledgements	3
iv.	List of Figures	6
v.	List of Abbreviations	8
vi.	Abstract	9
1.	Introduction	10
1.1	Theory	13
1.1.1	Erosion in Ductile Materials.....	13
1.1.2	Flow Disruption.....	14
1.1.3	Stress Concentration Distribution.....	16
1.1.4	Substrate Surface Hardness.....	17
1.1.5	Erosion Modeling.....	18
2.	Simulation Methodology	21
2.1	Computational Problem Statement	21
2.2	CAD Modeling	21
2.3	Meshing	23
2.4	Setup	24
2.4.1	Turbulence Modeling	24
2.4.2	Discrete Phase Modeling	25
2.4.3	Materials, Boundary Conditions and Initialization	26
2.5	Experimental Validation	27
2.5.1	Materials and Methods	27

2.5.2	Submerged Water Jet Erosion Setup	28
3.	Results and Discussions	29
3.1	Validation Experiment	29
3.2	Microchannel Depth Variation	30
3.3	Microchannel Cross Sectional Shape Variation	31
3.4	Surface Pattern Variation	32
3.5	Discussions	33
4.	Conclusion	35
5.	References	36

iv. List of Figures

Figure Number	Description
Fig. 01	<i>Graphical representation of the depth variation and hydrodynamic pressure variation over the material's surface. [Perez, 2019]</i>
Fig. 02	<i>Schematic showing the Ductile and Brittle Erosion mechanisms.</i>
Fig. 03	<i>Schematic showing the possible impinging particle rebound trajectories.</i>
Fig. 04	<i>Illustration of Longitudinal Flow (Left) and Cross Flow (Right).</i>
Fig. 05	<i>(Row 1) CAD Model of the untextured substrate before meshing. (Row 2) Dimensions of the Base Substrate and Impinging Jet. (Row 3) Square-Shaped Microchannel patterns with Depth variation. (Row 4) Microchannel patterns with Cross-Sectional Shape Variation. (Row 5) Texturing pattern variation.</i>
Fig. 06	<i>Solution Convergence on ANSYS Fluent 2022 R1.</i>
Fig. 07	<i>Graphical Representation of the Experimental and Simulated Results of the erosion rates with different erosion models.</i>
Fig. 08	<i>(Left) Eorion Contour Plots for the untextured substrate validation experiment. (Right) Particle Pathline tracking for the untextured substrate.</i>
Fig. 09	<i>Graphical Representation of the change in Erosion Rates observed, with a variation in Microchannel Depth.</i>
Fig. 10	<i>Graphical Representation of the change in Erosion Rates observed, with a variation in Microchannel Cross-Section Shape.</i>

Fig. 11

Graphical Representation of the change in Erosion Rates observed, with a variation in Surface Patterns.

Fig. 12

Velocity Coloured Pathline Figures of the DPM Particles striking the surface and depicting rebounding within the surface textures at different trajectories for different samples. (Marked in Red)
(Top Left) 0.3mm Depth Square Section Microchannels
(Top Right) 0.6mm Depth Square Section Microchannels
(Bottom Left) 0.5mm Depth V Section Microchannels

Fig. 13

Generic Erosion Rates coloured contour figures of the textured substrates correlating stress concentration and material loss.
(Top Left) 0.5mm Depth Square Section Microchannels
(Top Right) 0.6mm Depth Square Section Microchannels
(Bottom Left) 0.5mm Depth V Section Microchannels

v. List of Abbreviations

Abbreviations	Description
<i>AM</i>	Additive Manufacturing
<i>CAD</i>	Computer Aided Design
<i>CFD</i>	Computational Fluid Dynamics
<i>DI</i>	De-Ionized
<i>DPM</i>	Discrete Phase Model
<i>RANS</i>	Reynolds Averaged Navier Stokes Equation
<i>SFE</i>	Stacking Fault Energy
<i>SS</i>	Stainless Steel
<i>SST</i>	Shear Stress Transport

vi. Abstract

Across industries, we always tend to look to nature to understand how to tune and optimize our solutions to make them more efficient. This is what we did when faced with the challenge of minimizing the erosion rates observed on surfaces in marine environments. With this project we try to understand how surface textures can be tuned to change the erosion mechanisms in play to minimize the overall erosion rates, using Computational Fluid Dynamics (CFD). Different types of textures were explored and the Depths and Cross-Sectional Shapes were varied and explored to understand their effects on the erosion rates. The simulation was modeled, meshed, set up and run using Ansys Fluent and Workbench 2022 R1. Validation was done by comparing the experimentally determined Submerged Slurry Erosion values on polished SS316L substrates and the simulation values using 4 different erosion models, Generic, Finnie, McLaury and Oka. With this, we were able to explore the erosion rate variations with different parameters and understood the mechanisms and limitations of each. We were able to obtain optimum values for the three parameters under study, with the 0.6mm texture depth, V-shape cross section and Microchannels showing the lowest erosion rates. We observed a reduction in the erosion rates by almost 58% in some cases. This can be attributed to the different erosion mechanisms taking place on the surface of the substrate, along with factors such as flow disruption, stress concentration distribution on the surface, and increased hardness playing a very important role in deciding the overall erosion rates.

1. Introduction

The quest to optimize surfaces and bulk substrates to achieve the most optimal performance for an array of applications has always been at the forefront of Material Sciences and Engineering. Over the entire life cycle of a component, the body is periodically and cyclically exposed to various environmental and operating conditions which may deteriorate its performance over time due to a number of reasons, be it fracture, fatigue, wear, creep, apart from the forces the component was designed to withstand. For any item of equipment, there is a critical minimum level of performance. A mechanical degradation proceeds at a rate that varies with local conditions and failure occurs if the performance declines to below the critical level. This eventually leads to material degradation, resulting in the decreasing performance of the component and eventual component failure. Out of all the parameters and forces that the component experiences throughout its lifestyle, Engineering Sciences teaches us that there are only a handful of forces that we can optimize and control, and we do this indirectly by tuning various mechanical, tribological, optical, and/or the crystallographic properties of the substrate.

Wear tends to be an unavoidable result when any type of relative motion (Translational/Rotational Motion) exists between solid bodies, irrespective of the magnitude involved. Surface Roughness too, fundamentally plays a very important role in determining the material loss under various testing conditions, purely due to the non-uniformity of the height of the surface layer, because of the asperities and valleys and general surface geometry cause intense physical and tribological interactions between the two surfaces. Artificial techniques are available to modify or reduce the surface roughness via polishing, but then again we never will really reach a truly smooth flat surface. Wear adversely affects the components life cycle and efficiency, may also severely damage the component, and increase overall maintenance costs.

Erosion is a mechanical phenomenon that occurs when solid particles strike the surface repeatedly. Repeated particle collisions on a ductile surface will result in the creation of craters and platelets; craters will enlarge with each subsequent particle impact, while platelets will finally be easily removed into the flow. Under sand particle impact, brittle material will develop lateral and radial cracks, which will proliferate and eventually form small pieces that are removed by continuous solid particle impingement. Surface engineering is a relatively new field that deals with challenges that arise from the surface of engineering components.

The exterior of a component is often thought to be significantly most vulnerable and prone to damage than the interior. Most tribological material degradation phenomena play out on the surface of the substrate, hence making it all the more necessary to understand what parameters of the substrate and its surface can we optimize. With parametric studies like these, it becomes difficult to experimentally determine an optimum texture, hence we make use of numerical models and simulations to confirm our hypothesis.

Computational Fluid Dynamics (CFD) is the process of mathematically simulating fluid flows and studying flow characteristics in order to understand the numerous dynamics that play out in each numerically calculated setting. The calculations necessary to model the free-stream flow of the fluid and the interaction of the fluid (liquids and gasses) with surfaces determined by boundary conditions are performed on computers. Better answers can be achieved with high-speed supercomputers, which are frequently required to handle the largest and most complicated issues.

The mathematical model changes depending on the problem, such as heat transmission, mass transfer, phase change, chemical reaction, and so on. Furthermore, the accuracy of a CFD study is heavily dependent on the process's overall structure. The verification of the mathematical model and data is extremely important to create an accurate case for solving the problem. We used Ansys Fluent and Ansys Workbench Student 2022 R1 for all the CFD modeling involved in this project.

In the Minor Project, we worked on trying to theorize various erosion mechanisms which may play out under different conditions, and subsequently affecting the overall erosion rate. This experimentation was carried out with textured samples. Texturing happened via imprinting, using a wire mesh mold under applied hydraulic load for 10 mins. Conventionally vs Additively manufactured samples were also compared with each other to understand how their erosion and corrosion rates vary. From the study, we were able to confidently state our observations as follows:

- Textured samples showed much lower observation rates than the untextured, as-received samples, indicating that there are indeed other mechanisms playing out which affect the overall erosion rates (represented in mm^3/hr). In some cases, there was almost a 40% reduction in erosion rates observed. One main conclusion was that this could be attributed to the increase in localized stress concentrations on the edges

of the substrate which may easily fracture and contribute directly to material loss and the overall erosion rates. Textured substrates also have higher corrosion rates than untextured samples, which can be directly accounted for by the increase in the surface area of the substrate with texturing.

- We were able to verify the variation of erosion rates with impinging angles, indicating it to be one of the most important deciding factors in determining the overall erosion rates. Similar variations were observed in both Conventionally and Additively manufactured samples. 30° impinging angles show higher erosion rates than 90° impingement angles, which can be accounted for by the different erosion mechanisms which play out in the different cases, plastic deformation vs abrasive wear and chipping.
- Additively Manufactured samples show much higher corrosion rates when compared to conventionally manufactured substrates.

Additionally, previous literature tells us the importance of surface textures, indicating the multiple tribological benefits it has including promoting lubrication, reduced friction and wear etc. It was also reported that surface texturing promotes lower hydrodynamic pressures during fluid-solid interactions and even increased load bearing capacity of the substrates, due to increased hardness as a result of the texturing process. The wear mechanisms which take place within the textures during these slurry flows however are of special interest to us. With the addition of surface textures, certain newer erosion parameters and mechanisms, such as stress concentration distribution across the surface and the Flow Disruption within the textures also play an important role in determining the governing erosion mechanism.

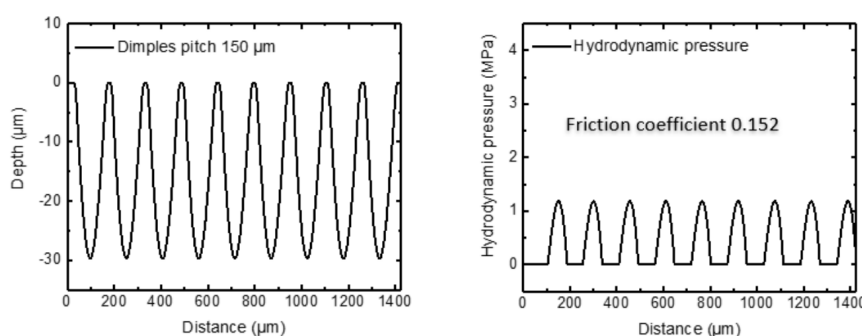


Fig. 01 Graphical representation of the depth variation and hydrodynamic pressure variation over the material's surface. [Perez, 2019]

In this project hence, we look at using CFD Modeling to understand the influence of Surface Textures on erosion wear. CAD Modeling is done using SpaceClaim 2022 R1 on the Ansys Workbench to create surface textures with different parameters, exploring variations in Texture Depth, Cross-Sectional Shape and Pattern Type. These models were then meshed and the simulation was set up. Erosion rates were compared using contour plots of the surface available, however Ansys Fluent Erosion Modeling gives us a choice between 4 different erosion models, the Fluent Standard Erosion Model, Finnie Erosion Model, McLaury Erosion Model and Oka Erosion Model. With our validation experiment, we were able to compare the experimentally obtained and the simulation results to understand which model we could expect the most accuracy with. The validation experiment consisted of a Submerged Water Jet Erosion setup with the substrate being completely submerged and subject to a slurry jet for 1 hour. The mass loss and erosion rate data was calculated from the same. Finally, with the simulation validated, we could proceed using the similar simulation setup with all the different surface textures previously modeled and compare their results.

1.1. Theory

Material erosion as the result of the impact of solid particles is a discrete and cumulative process involving prolonged periods of exposure under steady state or variable conditions. This form of wear is a complex phenomenon consisting of several simultaneous and interactive processes. Variables affecting the erosion can be broadly broken down into three types: impingement variables describing the particle flow, particle variables and material variables. The impingement variables are particle velocity, impact angle and particle concentration. Particle variables include particle shape, particle density and particle size. Material variables include all the target material mechanical properties Young's modulus, Poisson's modulus, the hardening behavior and the microstructure, the hardness and the toughness.

1.1.1. Erosion in Ductile Materials

The particle velocity can be resolved in two components, one normal to the body surface and another parallel to it. The normal component is responsible for the particle penetration into the substrate surface while the parallel one gives the particle scratching action. Depending on whether the particle velocity parallel to the body becomes zero during the collision, two expressions of the volume of material removed by cutting wear can be evaluated.

This model was based on the assumption that the erosion mechanism is a process of micro-cutting in which the surface material is removed in the form of cuttings. Particles striking the surface at low impact angles form a crater. Material is then continually removed by further particle impacts. Particles impacting a surface at larger angles will result in the surface material being piled up. This raised material is then removed by further particle impacts.

As mentioned above, with the addition of surface textures, when compared to an untextured substrate we can confidently say that there are multiple additional mechanisms and factors which dictate the overall erosion rates. Some of these factors are discussed below. Brittle material on the other hand, will grow lateral and radial cracks under sand particle impact, which will grow and eventually form small pieces that are removed by continuous solid particle impingement.

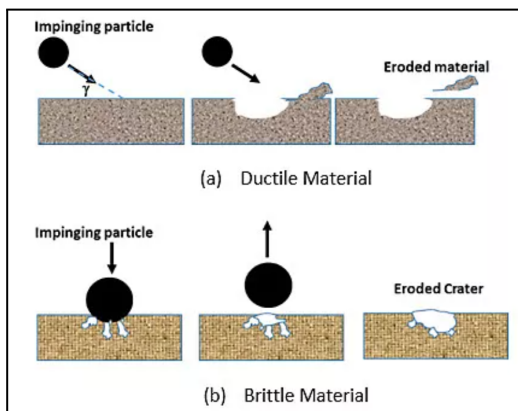


Fig. 02 Schematic showing the Ductile and Brittle Erosion mechanisms.

1.1.2. Flow Disruption

We understand that with fluid flows near corners and edges of the substrate texture with sufficient velocity, we can expect the recirculating fluid flow fields within the structures. The grooves in fact enhance this rotating flow, similar to the generation of viscous eddies. This rotating flow can drastically affect the impact velocity and direction of motion of the impinging particles.

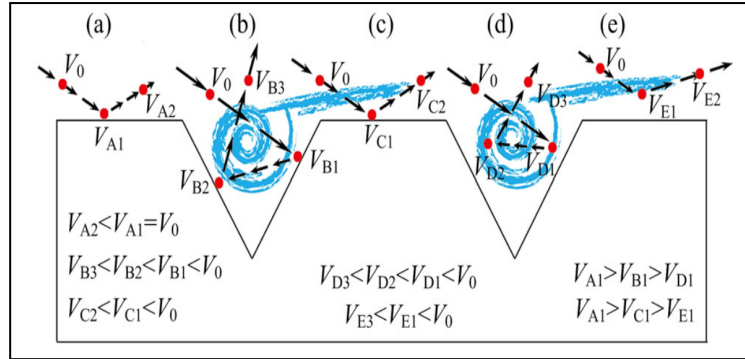


Fig. 03 Schematic showing the possible impinging particle rebound trajectories.[6]

Let us consider an untextured surface subject to an impinging slurry jet. On impact, the magnitude of energy transfer that occurs during the inelastic collision with the surface would be much higher due to the unchanged, undisrupted state of the impinging particle. However if we compare this with a textured surface, irrespective of the features of the texture, we can confidently say that it will definitely disrupt the flow field. The rotating fluid flow as the result of the grooves essentially creates an air cushion and slows down the subsequent impact velocity of the particle [6].

We understand that the flow field on the surface of the substrate can be split up into two components, the longitudinal and the cross flow profiles, whose origin is not the same as shown in the figure below. For the longitudinal flow, the origin is much deeper in the groove than the origin of the cross flow, which is located closer to the upper tip of the groove. The cross flow components are generated by the longitudinal vortices and other near surface events. In a turbulent boundary layer, the viscous sublayer flow would change its direction on interaction with the surface geometry. These turbulent events which comprise lateral flow velocity constituents are displaced farther away from the surface due to the higher elevation of the cross flow origin. This displacement results in a thicker viscous sublayer and hence lower wall shear stress, i.e., decreased drag.

Thus, we can assume that one of the important features for a drag reducing surface is the difference in height of longitudinal and cross flow origins. The basic action that textures are assumed to exert is a damping of the crossflow vortices that accompany the turbulent flow. In this way they affect a reduction of the near-wall level of turbulence, and thus of the eddy viscosity and ultimately of the drag. Texture Height Difference and Shape are hence very important in determining the fluid flow interaction.

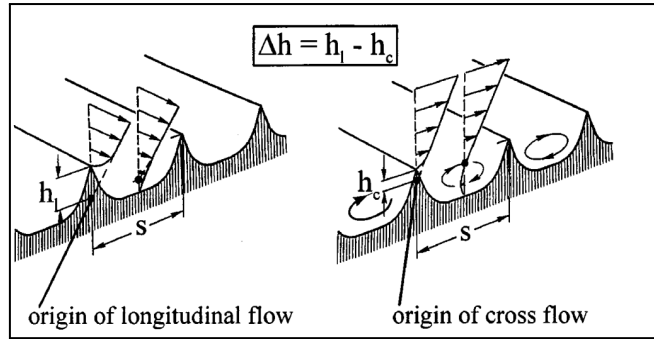


Fig. 04 Illustration of Longitudinal Flow (Left) and Cross Flow (Right).

Energy balance during impact showed that at least 90% of the initial kinetic energy of the particle is dissipated in plastic deformation in the target, meaning that the rebounding particle has less than 10% of the initial kinetic energy it had, all lost during the first elastic collision with the target surface. For the impinging fluid particles, due to the abrupt change in flow direction and subsequent loss of momentum, the energy with which it finally collides with the substrate is significantly lesser than the energy of the fluid particles straight from the impinging jet, with comparatively does result in lower overall erosion rates. Hence important texture parameters such as Texture Depth and Cross Section shape are very important in understanding fluid flow interactions.

1.1.3. Stress Concentration Distribution

The stress concentration distribution across the surface of the substrate is very important in understanding not directly the erosion mechanisms which occur, but in computing the overall erosion rates. Erosion rates are experimentally calculated as the mass loss over the duration of the experiment divided by the density of the substrates. As a direct consequence of surface concentrations, the quantum of material loss would increase and hence the erosion rate, thereby making it critical to minimize the stress concentrations on the surface of the substrate.

Stress concentrations are certain areas on an object where by virtue of its surface geometry, the stress is significantly greater here than in the surrounding areas. This occurs mainly on sharp edges, grooves, holes or other areas where abrupt discontinuities in surface geometry exist. The stress in these areas is generally much more which can be accounted for by the forced convergence of internal force lines near these regions due to its geometry. For ductile materials such as Stainless Steel, increased loads may cause localized plastic deformation (such as fatigue cracks) which would initiate in sites with higher stress concentration,

allowing for a redistribution of stress so that the component can continue to sustain the load. Once a crack is initiated in one of these sites however, we must consider the additional stress concentrations which arise as a result of the irregular geometry of the crack. The crack will also grow and propagate if the energy needed for it to do so is sufficient enough to overcome the resistance of the material. Once the threshold toughness for crack initiation is crossed, the required energy for crack propagation is so low that it can even be provided by the energy transfer which occurs when the elastic particle collisions occur on the surface of the substrate.

In order for us to understand how big of a factor the stress concentration actually is in determining the erosion rates, we had to look at the two main factors which influence this, the Cross-Sectional Shape of the texture and the Patterning Type which has occurred. Exploring the Shape Factor, we compared 3 surface textures with different cross-section shapes, namely a Base Untextured Substrate, a Square-Shaped Microchannels and V-Shaped Microchannels. Due to the increased number of edges, the Square-shaped Microchannels has the highest stress concentration, much more than that of the V-shaped Microchannels which inturn would still have higher stress concentrations than the base substrate, assuming all samples are subjected to similar pre-processing methods. Similarly when comparing Pattern Type, we are actually looking at two regular patterns, Microchannels and Microcavities, once again the Microcavity patterned substrate due to a higher number of edges would have a much higher stress concentration than the Microchannel patterned substrate.

1.1.4. Substrate Surface Hardness

The surface hardness of the remains one of the most dominating factors which affect the erosion mechanisms and overall rates, apart from impact velocity and impinging angles. The surface hardness of the textured substrate increases during patterning (imprinting) due to the introduced surface compressive stresses.

An increase in hardness provides resistance to penetration and should, therefore, result in lower erosion rates. There is however an upper limit to how much we can increase the surface hardness, as after a point the material will succumb to cracks and subsequent fracture via the Brittle Erosion Mechanism. In addition it has been noted that the polymorphic materials have low stacking fault energy (SFE) planar slip modes and high work hardenability, and that these factors are empirically found to be beneficial for erosion resistance. A low stacking fault

energy implies a wide separation of partial dislocations to cross slip. This difficulty translates into relatively lower recovery rates, which results in lower erosion [20].

1.1.5. Erosion Modeling

Ansys Fluent gives its users primarily the choice between 5 different erosion models when simulating Discrete Phase Modeling (DPM) Erosion, namely the Generic (Default), Finnie, McLaury and Oka models. Each of the above models use a different mechanical model to try and accurately predict the erosion rate at the end of the experiment, taking into account different parameters and empirical constants for the same. The Finnie erosion model is more suited for ductile materials, where the erosion varies with the impact angle and velocity. The Oka model provides a more realistic correlation by including the effect of wall material hardness and is widely used in theoretical erosion models. The McLaury erosion model was developed to predict the erosion rate of solid particles in water; it has been primarily used in slurry flows [21].

The Ansys Fluent Standard Erosion Model (Generic) is given by:

$$R_{Erosion} = \sum_{p=1}^{N_{Particles}} \frac{m_p C(d_p) f(\alpha) v^{b(v)}}{A_{Face}}$$

$$f(\alpha) = 0 + 22.7\alpha - 38.4\alpha^2 ; \alpha \leq 0.267 \text{ rad}$$

$$f(\alpha) = 2 + 6.8\alpha - 7.5\alpha^2 + 2.25\alpha^3 ; \alpha > 0.267 \text{ rad}$$

Where $C(d_p)$ is the particle diameter function, m_p is the mass flow rate, $f(\alpha)$ is the impact angle function, v is the impact velocity and $b(v)$ is the velocity exponent. A_{Face} is the total contact face area.

The Finnie Erosion Model is given by:

$$Q = \frac{mV^2}{\rho\psi K} \left(\sin 2\alpha - \frac{6}{K} \sin^2 \alpha \right) \quad \tan \alpha \leq \frac{K}{6}$$

$$Q = \frac{mV^2}{\rho\psi K} \left(\frac{K \cos^2 \alpha}{6} \right) \quad \tan \alpha > \frac{K}{6}$$

Where Q represents the volume of material eroded by a single abrasive grain, m is the mass of the single particle, p is the plastic flow stress of the material, α is the impinging angle, V is the particle velocity, Ψ is the ratio of depth of contact to depth of cut and k is the ratio of the vertical to horizontal force components on the particle.

The McLaury Erosion Model is given by:

$$E = A V_p^n f(\gamma)$$

where

$$A = F B h^n (\gamma)$$

$$f(\gamma) = b\gamma^2 + c\gamma \quad \text{for } \gamma \leq \gamma_{lim}$$

$$f(\gamma) = x \cos^2 \gamma \sin(\omega \gamma) + y \sin^2(\gamma) + z \quad \text{for } \gamma > \gamma_{lim}$$

Where E is the erosion rate, F is an empirical constant, V_p is the particle impact velocity, Bh is the Brinell Hardness Number, n is the exponent and $f(\gamma)$ is the impact angle function. F, b, c, x and y are experimental constants in this case.

The Oka Erosion Model is given by:

$$E = E_{90} \left(\frac{V}{V_{ref}} \right)^{k_2} \left(\frac{d}{d_{ref}} \right)^{k_3} f(\gamma)$$

$$f(\gamma) = (\sin \gamma^{n_1}) (1 + H_v (1 - \sin \gamma))^{n_2}$$

Where E, V and d are the overall erosion rates, particle impact velocity and diameter respectively, and E_{90} , V_{ref} and d_{ref} are the erosion rates at 90° impinging angle, and the corresponding reference impact velocity and particle diameter under those conditions. $f(\gamma)$ is the impact angle function, γ is the impinging angle, H_v is the Vickers Hardness and n_1 and n_2 are impact angle function exponents.

2. Simulation Methodology

2.1. Computational Problem Statement

Submerged Slurry Simulations were set up on ANSYS Fluent to understand the erosion resistance of substrates with different surface textures. The computational domain to simulate our Submerged Slurry Erosion setup is shown as in Figure 04. There are 3 main domains considered in this setup, the Air Domain, Water Domain and the Substrate itself. The air domain is modeled as a cuboid with dimensions (15 x 7.5 x 7.5mm) and is enclosed with Air (Fluid). The water domain is marked as the nozzle supplying the impinging jet, containing a mixture of Water and abrasive particles (Particle Parameters in brief) simulated with a Discrete Phase Model (DPM) with defined injection parameters. The substrate is a 10mm x 10mm x 5mm cuboid made of Stainless Steel SS316L (Density: 8000 Kg/m³). Various substrates are modeled on SpaceClaim R1 2022 with varying texturing parameters. Our objective with this simulation is as follows:

- Compare different Mathematical Erosion Models available on ANSYS Fluent to understand how accurately an experimental Submerged Slurry Setup can be simulated.
- Compare different texture heights to understand how a height variation affects the overall erosion rates.
- Compare different regularly textured substrates with channel shapes to understand how a cross sectional variation affects the overall erosion rates.
- Compare different surface patterns to understand how they affect the overall erosion rates.

2.2. CAD Modeling

The Base Substrates (Textured and Untextured) were all modeled on SpaceClaim 2022 R1 before being exported for Meshing and subsequently analysis. Substrates of 10mm x 10mm x 5mm were modeled as a rectangular solid, with an Air Enclosure of dimensions 25mm x 25mm x 15mm, with 10mm Standoff Distance, additionally designated to understand the flow lines of the slurry jet over the stand off distance. The Nozzle was further designated as a solid cylinder with designated (Velocity Inlet) and Nozzle Outlet as the interface between the tip of the cylinder and the surface of the Air Enclosure Domain.

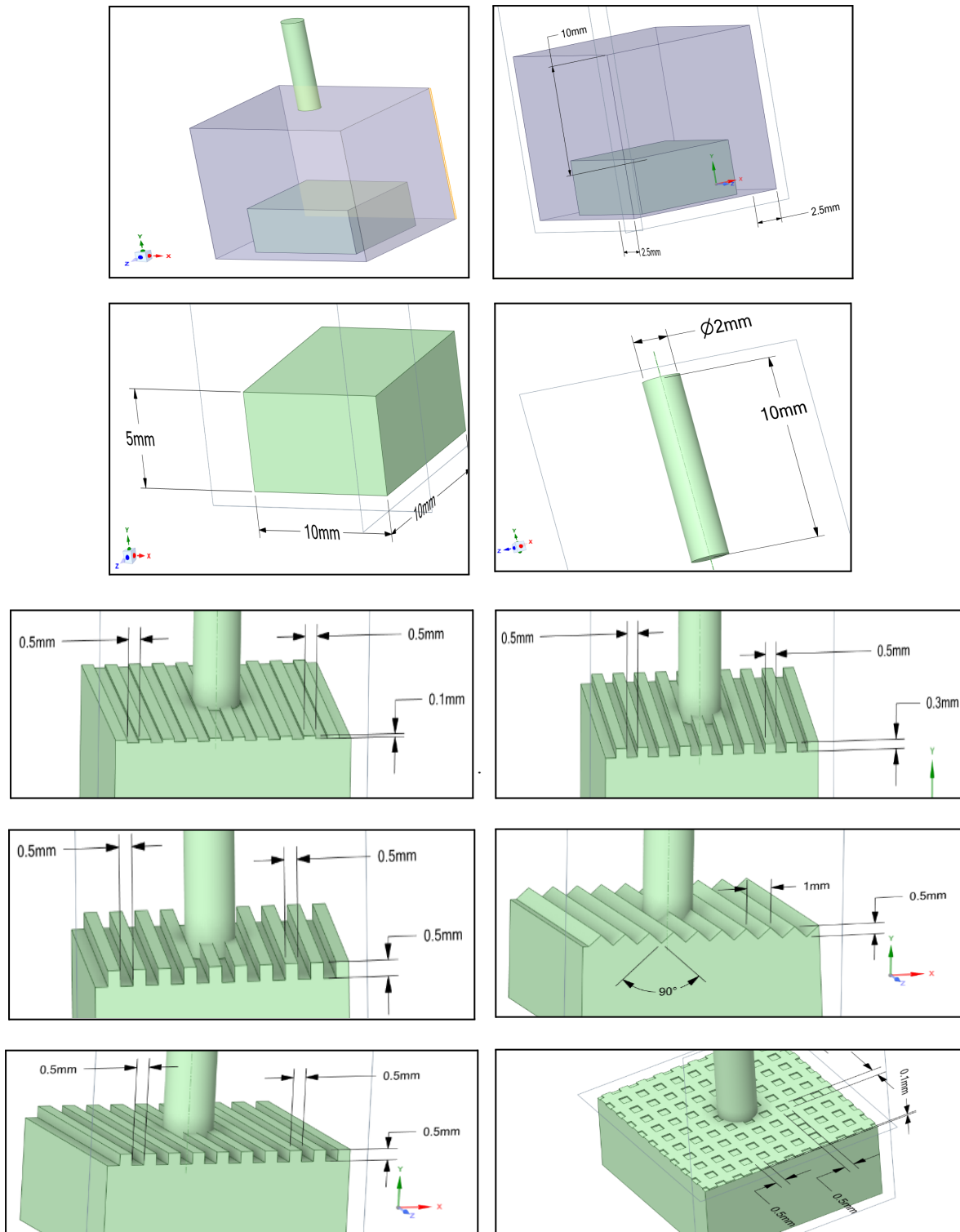


Fig 05. (Row 1) CAD Model of the untextured substrate before meshing.

(Row 2) Dimensions of the Base Substrate and Impinging Jet.

(Row 3) Square-Shaped Microchannel patterns with Depth variation.

(Row 4) Microchannel patterns with Cross-Sectional Shape Variation.

(Row 5) Texturing pattern variation.

The entire nozzle is later designated as the Fluid Domain. The patterns modeled on SpaceClaim with various surface textures are listed below:

Sample Code	Pattern Type	Texture Depth (mm)	Cross-Section Shape
T0	Untextured	-	-
T1	Microcavities	0.1	Square Shaped
T2	Microchannels	0.1	Square Shaped
T3	Microchannels	0.3	Square Shaped
T4	Microchannels	0.5	Square Shaped
T5	Microchannels	0.6	Square Shaped
T6	Microchannels	0.7	Square Shaped
T7	Microchannels	0.5	U - Shaped
T8	Microchannels	0.5	V - Shaped

2.3. Meshing

After the CAD Model is imported into the Meshing window automatically via the Ansys Workbench, and first the main named sections are declared here. These are listed out as below:

- Inlet Named Section: The top end of the cylinder modeled as the Nozzle.
- Outlet Named Section: The interface between the bottom end of the cylinder modeled as the Nozzle, and the top surface of the Air Domain.
- Air Domain Named Section: Cuboid to represent the fluid trapped within the air enclosure during the Submerged Slurry simulation.
- Fluid Domain Named Section: Entirety of the cylinder modeled as the Nozzle.

Succeeding this only did we proceed for the actual meshing of the entire setup (Substrate, Air and Fluid Domain). Meshing happened with a CFD Fluent Solver Preference of Linear Order Size with the following meshing results for the validation simulation; Number of Elements as 27249, Nodes as 22791 with a 0.3mm Element Size. A mesh independence study was also carried out before exporting the meshing data to the Fluent setup.

2.4. Setup

The Fluent Launcher 2022 sets up the experiment on Fluent 2022 R1. We choose Double Precision with Displaying the Mesh After Reading. 4 Solver processes run parallelly on the local machine with 0 GPUs in use. The Console available during setup shows us the backend transfer and setup of files, imported from meshing. A pressure-Based solver type is used in these simulations with Absolute Velocity Formation and Steady Time. As with all our experimental cases, Gravity was accounted for with 9.81 m/sec² along the y-axis.

2.4.1. Turbulence Modeling

Navier Stokes is the governing equations for all solutions generated by Computational Fluid Dynamics (CFD), however a modified version of this model called the Reynolds Averaged Navier Stokes Equations (RANS Equations) used primarily to describe turbulent flows are both listed below. With this model, the results that we get are now approximate time averaged solutions to the setup. This however is applicable only to Incompressible Newtonian Fluids. The equations represent a balance between the change in mean momentum of a single fluid element due to the unsteadiness and convection of the mean flow field, with the Body Force, Isotropic Stress, Viscous Stress and Reynolds Stress. The last term in the equation defines the Reynolds Stress which is non-linear and needs to be solved for. For this various Turbulence models are used such as the SST, K- ω and K- ϵ models. For our setup, the 2 equation Realizable K- ϵ model was chosen with scalable wall functions which are used to primarily model the ‘near wall treatment’ of the fluids. Walls are a major source of turbulence and scalable wall functions help model the fluid behavior as it approaches the wall. The Navier Stokes and RANS equations are as follows:

$$\frac{\partial \rho}{\partial t} + \frac{\partial}{\partial x_i} (\rho u_i) = 0$$

$$\frac{\partial}{\partial t} (\rho u_i) + \frac{\partial}{\partial x_j} (\rho u_i u_j) = \frac{\partial \rho}{\partial x_i} + \frac{\partial}{\partial x_j} \left[\mu \left(\frac{\partial u_i}{\partial x_i} + \frac{\partial u_j}{\partial x_i} - \frac{2}{3} \delta_{ij} \frac{\partial u_i}{\partial x_i} \right) \right] + \frac{\partial}{\partial x_j} (-\rho u_i u_j)$$

The Standard K- ϵ model is based on model transport equations for the turbulence kinetic energy (K) and its dissipation rate (ϵ). In the derivation of the Standard K- ϵ model, the assumption is that the flow is fully turbulent, and the effects of molecular viscosity are negligible. The standard model is therefore valid only for fully turbulent flows. The calculations are governed by the following equations for K and ϵ respectively.

$$\frac{\partial}{\partial t} (\rho k) + \frac{\partial}{\partial x_i} (\rho k u_i) = \frac{\partial}{\partial x_j} \left[\left(\mu + \frac{\mu_t}{\sigma_k} \right) \frac{\partial k}{\partial x_j} \right] + G_k + G_b - \rho \varepsilon - Y_m + S_k$$

$$\frac{\partial}{\partial t} (\rho \varepsilon) + \frac{\partial}{\partial x_i} (\rho \varepsilon u_i) = \frac{\partial}{\partial x_j} \left[\left(\mu + \frac{\mu_t}{\sigma_k} \right) \frac{\partial \varepsilon}{\partial x_j} \right] + \rho C_1 \frac{\varepsilon}{k} (G_k + C_3 G_b) - \rho C_2 \frac{\varepsilon^2}{k} + S_\varepsilon$$

$$\mu_t = \rho C_\mu \frac{k^2}{\varepsilon} \text{ and } C_\mu = \frac{1}{A_o + A_S \frac{kU^*}{\varepsilon}}$$

The term “realizable” means that the model satisfies certain mathematical constraints on the Reynolds stresses, consistent with the physics of turbulent flows. The Realizable K- ε further differs from the Standard K- ε model in two important ways:

- The Realizable K- ε model contains an alternative formulation for the turbulent viscosity. In this case, the μ_t term (Eddy Viscosity) is computed more accurately.
- The C_μ term is not treated as a constant like it is in the Standard K- ε Model, instead it is formulated and computed to model the turbulent flow more accurately. C_μ represents a function of Average Strain, Rotation Rates and Angular Velocity.

2.4.2. Discrete Phase Modeling

The Discrete Phase is set to interact with the continuous phase, with the DPM Sources to be updated every single flow iteration. The maximum number of steps is set as 2500 and with High-Res Tracking. As for Physical Models, Virtual Mass Force (Virtual Mass Factor 0.5), Pressure Gradient Force and Erosion/Accretion were selected. The injection is named and is set up as Injection Type and the Inlet named section is selected as the Injection Surface. The particle is selected as Massless types with uniform diameter distribution and is Injected Using Face Normal Direction. The Point properties are shown below. These values remain constant in all simulations as Boundary Conditions. For Point properties, the Diameter is set as 1.5e-05m, velocity set as 20 m/s and Total Flow Rate as 0.0003 Kg/sec.

Ansys Fluent calculates the trajectory of a discrete phase particle by integrating the force balance on the particle, which is done in a Lagrangian frame. This force balance equates the particle inertia with forces acting on the particles such as drag, pressure, buoyancy and added mass or virtual forces. The force balance equation for the impinging particles is as follows

$$\frac{\partial \bar{u}_p}{\partial t} = F_D (\bar{u} - \bar{u}_p) + \frac{\bar{g}(\rho_p - \rho)}{\rho_p} + \bar{F}$$

where,

$$F_D = \frac{18\mu C_D Re}{24 \rho_p d_p^2}, Re = \frac{\rho_p d_p |\bar{u} - \bar{u}_p|}{\mu} \text{ and } \bar{F} = C_{vm} \frac{\rho}{\rho_p} \left(\bar{u}_p \Delta \bar{u} - \frac{\partial \bar{u}_p}{\partial t} \right)$$

A large number of particles are tracked in the field after obtaining a converged flow solution. In this approach, the particles are modeled as a point mass that does not affect the flow. The particle-particle interaction is also neglected in the standard formulation of DPM. It is possible to incorporate the effect of the discrete phase on the continuum and achieve a two-way coupling, allowing interaction between the phases. This is accomplished by alternately solving the discrete and continuous phase equations until the solutions in both phases have stopped changing. Spherical Drag law formulation is used in evaluating the Drag Coefficient C_D for smooth particles. We can assume the impinging particles would take a spherical shape after multiple iterations of the recirculating flow. a_1 , a_2 and a_3 are all constants which apply over several ranges of Reynolds Number Re .

$$C_D = a_1 + \frac{a_2}{Re} + \frac{a_3}{Re^2}$$

2.4.3. Materials, Boundary Conditions and Initialization

For our material selection, for the Air Domain, the material name is set as “water-liquid”, Fluid Domain as “water-liquid” and the Substrate as “steel”. With the Boundary Conditions, velocity inlet was set at the Inlet Named Section, with Momentum Conditions as detailed further. Velocity Specification Method was done with the Magnitude, Normal to Boundary option with an Absolute Reference Frame and initial conditions of velocity at 20 m/sec and Gauge Pressure at 350000Pa (3 Bar). The Turbulence Conditions were specified with Intensity set at 5% and Viscosity Ratio set to 10.

The Inlet Named Section and Contact Region (Surface of the Substrate) have their Discrete Phase Model Boundary Condition Type as Escape and Reflect respectively, with polynomial Normal and Tangent Coefficient Components. Additionally for the Contact Region, Stationary Wall Conditions were chosen with No Slip Shear Condition and Standard

Roughness Model. The Normal and Tangential components of the Coefficients of Restitution of the particle on the target surface are given by the following equations:

$$e_{Perpendicular} = 0.988 - 0.78\theta + 0.19\theta^2 - 0.024\theta^3 + 0.027\theta^4$$

$$e_{Parallel} = 1 - 0.78\theta + 0.84\theta^2 - 0.021\theta^3 + 0.028\theta^4 - 0.022\theta^5$$

A pressure type outlet is set up at the Outlet Named Section with 0 Pa Gauge Pressure and set to Prevent Reverse Flow, with Escape Discrete Phase Type. A Standard Initialization is chosen, set to all the boundary conditions mentioned above and the simulation is then started at a 1s Pseudo Step Size until the convergence criteria is satisfied.

2.5. Experimental Validation

2.5.1. Materials and Methods

Our chosen substrate material is Stainless Steel SS316L (Density: 7800 Kg/m³), a Austenitic Steel alloy with Chromium (16-18%), Nickel (10-14%), Molybdenum (2%), Manganese (2%) and the rest trace elements, chosen due to its potential applications in various industries, specifically the marine industry, due to its intrinsic strength and corrosion resistant nature makes it highly durable. The high corrosion resistant nature of Stainless Steel can be attributed to its high Chromium content, which reacts on exposure to atmosphere forming Chromium Oxide (Cr₂O₃), a passive oxide layer which prevents further rusting of the substrate. The addition of Molybdenum also increases corrosion resistance by resisting local pitting and corrosive attack by the chloride ions and also increases its strength at higher temperatures. 316 Grade Stainless Steel is the most effective in very acidic environments. SS316L has been chosen instead of SS316 as the low Carbon content in the substrate means lesser deleterious carbide precipitation and it can be used extensively for medical applications.

Our substrate preparation involved first machining commercially available Stainless Steel SS316L to dimensions of 10 x 10 x 5 mm sample, further polished using Abrasive Polishing sheets of different grades (80, 220, 400, 600, 800, 1000, 1500, 2000) (Manufacturer: 3M). We then performed ultrasonication on our samples present in a Deionized (DI) water bath to get rid of any dust and debris for 10 mins at 35°C. All processes were carried out under highly

sterile conditions and Acetone (99.9%) was used primarily as our cleaning agent during processing. All testing and measurements were done under ambient conditions ($24 \pm 2^\circ\text{C}$ and relative humidity of around 35%) unless mentioned otherwise.

2.5.2. Submerged Water Jet Erosion Setup

Our Submerged Slurry Experiment, although having a very similar setup to a Classical Slurry Experiment, was set up as detailed. In an enclosed container, the SS316L untextured sample was held in place with a sample holder perpendicular to the direction of the impinging jet, with the impinging jet essentially striking the sample at a 90° angle, from a 2 mm diameter nozzle. A stand off distance of 10 mm was ensured in each iteration, at constant impingement velocity of 20 m/s. A closed loop ensures homogeneously distributed recirculating slurry fluid, with a concentration of 12.5 g of river sand per 2.5 L of water. A pulsating pump is used to circulate the slurry fluid at a pressure of 3.0 Bar and a mechanical stirrer is kept in the output cistern to ensure an even slurry distribution of sand and water. Rectangular samples of Stainless Steel SS316L were cut out and polished using During the experiment the water level in the enclosure such that the sample remained submerged and the nozzle dispensing the impinging jet just about contacts the surface of the water level.

99% pure Acetone was used as the cleaning agent and ultrasonication was performed before any weight measurement, where the sample was submerged in acetone and ultrasonicated for 5 mins at 30°C to get rid of any unwanted impurities. The experiment was run for 1 hour and then erosion rates were calculated via mass loss during experimentation.

3. Results and Discussions

3.1. Validation Experiment

The point or number of iterations after which a solution is deemed converged is subject to the simulation criteria. To identify the point of convergence, we look at monitoring the residual values of the simulation variables which directly quantifies the error in the solution of the given system of equations. The residual values monitor the variables in each control volume, mainly the continuity, momentum and turbulence variables residuals are tracked for convergence, as shown above. Each convergence plot represents the average of each variable for every iteration, normalized to a range from 0 to 1.

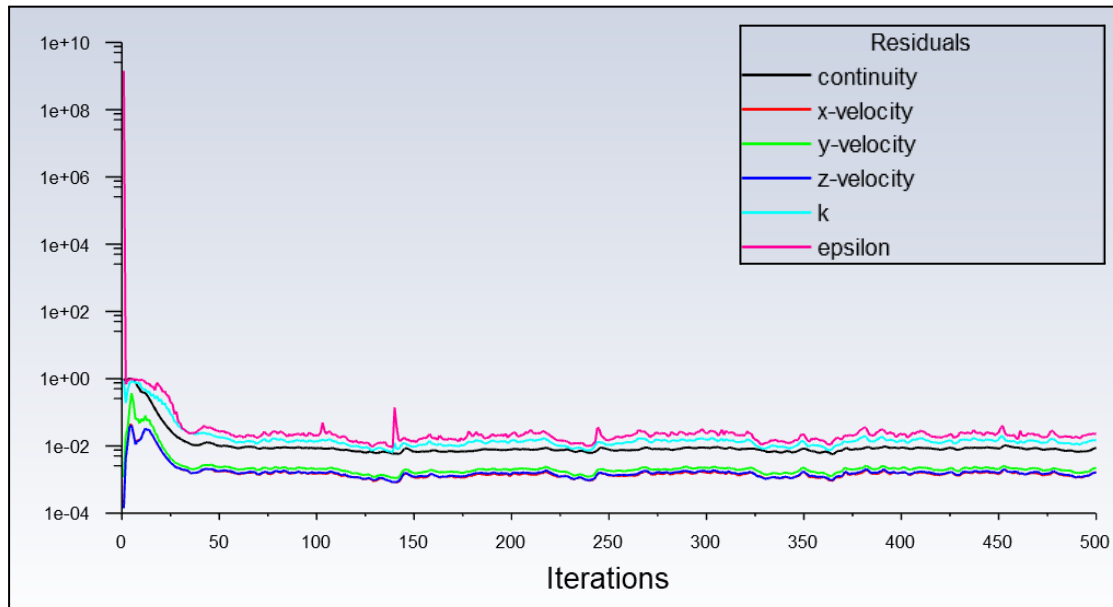


Fig. 06 Solution Convergence on ANSYS Fluent 2022 R1.

After collecting both the experimental and simulation data for the validation case (Base Untextured Substrate), we had to compare the results to test the accuracy of our setup and also to understand which of the four erosion models would be ideal for this analysis. The results of the validation experiment are shown below.

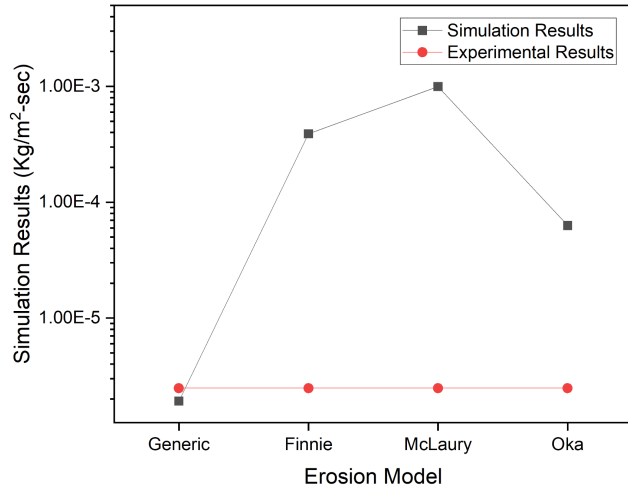


Fig. 07 Graphical Representation of the Experimental and Simulated results of the erosion rates with different erosion models.

We notice that the margin of error is lowest in case of the Generic (ANSYS Standard) erosion model, with the experimental erosion rate obtained as 2.48E-06 Kg/m²-sec and the Generic Model rate was 1.92E-06 Kg/m²-sec, which is an acceptable error margin in our case. Hence all further analysis is done comparing substrates using only the ANSYS Generic Fluent Erosion Model. The Pathline and Contour plots for the validation experiment are also shown below.

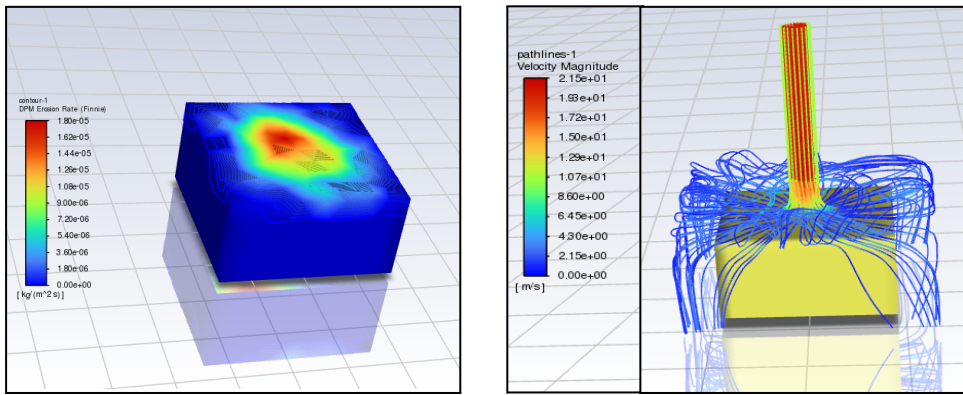


Fig. 08 (Left) Erosion Contour Plots for the untextured substrate validation experiment.
(Right) Particle Pathline tracking for the untextured substrate.

3.2. Microchannel Depth Variation

With a regular well defined surface texture geometry, we wanted to independently understand the effect that the depth of the microchannel has on the erosion rate of the substrate. For these tests, we compared the performance of six different samples, 5 textured with Square Cross

Section Microchannels of varying Depth (0.1mm, 0.3mm, 0.5mm, 0.6mm, 0.7mm) and an untextured Base Substrate. The results were collated and are as follows:

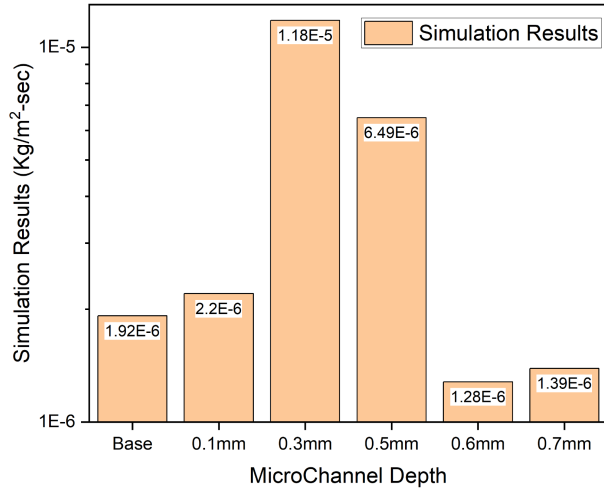


Fig. 09 Graphical Representation of the change in Erosion Rates observed, with a variation in Microchannel Depth.

We observe the extent to which the erosion rates have been affected by only varying the depth parameter. After tuning the depth of the texture, we see that the 0.3mm microchannel would indicate very different erosion mechanisms are playing out when compared to the 0.6mm microchannel. The 0.6mm and 0.7mm microchannel textures outperform the Base Substrate, with the 0.6mm microchannel showing erosion rates reduced by almost 33% which indeed is remarkable. We do observe the trend variation and that there in fact is an optimum value for a surface texture's depth parameter which would result in the lowest erosion rates. The height of the textures mainly determine the disruption and recirculation of the flowfield within the microchannels, thereby governing the energy and momentum exchange which takes place between the striking particles and the substrate.

3.3. Microchannel Cross-Sectional Shape Variation

The variation in cross-sectional shape is what would govern the trajectory of the impinging particle after it rebounds off the surface of the substrate. The impinging fluid flow field is disrupted by the presence of textures and results in changing erosion rates depending on the surface patterns. Stress concentration also determines the amount of material eroded which also is governed by the type of textures present. We compared the Base Substrate (Untextured), Square-Shape Cross Section and V-Shape Cross Section (both of equal depth) and observed the variation in erosion rates, which are listed below:

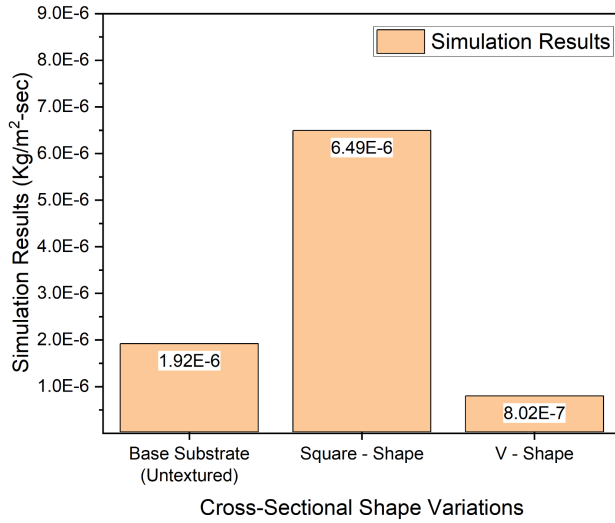


Fig.10 Graphical Representation of the change in Erosion Rates observed, with a variation in Microchannel Cross-Section Shape.

Once again, we note that surface texture cross section does play a big influence in tuning the erosion rates. The V-Shape sample tends to outperform both the Square-Shape and Untextured sample by more than 55%, due to its lower stress concentration compared to the Square-Shape sample, but also a different flow disruption pattern.

Additionally, due to the increase in stress concentration after patterning the Square-Shape sample, when erosion occurs, material will mainly be eroded from these areas of high stress concentration (edges), resulting in the increased erosion rates.

3.4. Surface Pattern Variation

We compared two different types of regular surface patterns, Microcavities and Microgrooves, both of similar depth and cross-sectional shape. Microcavities due to the increased stress concentration showed higher erosion rates than the untextured substrate but the microchannels due to an optimized flow field disruption tend to outperform the base substrate, showing lower erosion rates and better erosion resistance. It is also understood that the reservoir nature of the microcavities and the microgrooves imparts superior surface lubricative properties on the substrate. Microchannels will still show better lubricative properties as by design all trapped abrasive particles and debris have an outlet channel, as opposed to staying trapped within the cavities in the case of microcavities. The results are listed below:

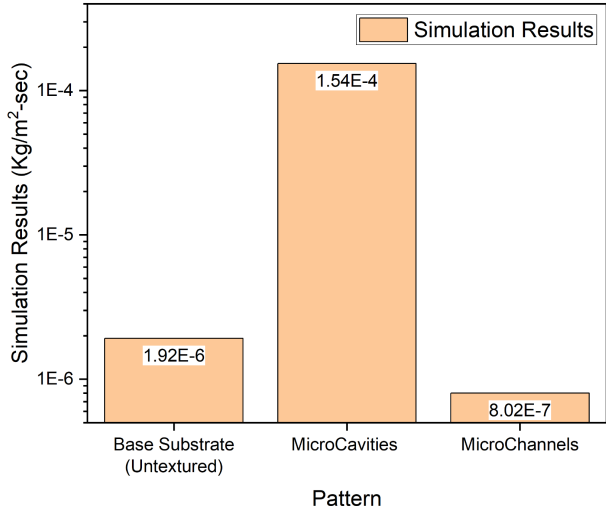


Fig. 11 Graphical Representation of the change in Erosion Rates observed, with a variation in Surface Patterns.

3.5. Discussions

As previously mentioned, the textures on the surface enhance the rotating flow, leading to the flow field disruption observed near the surface. This would directly affect the impact velocity and the subsequent mass loss associated with the substrate, due to the near surface interaction with the impinging jet, as observed with the change in velocity gradient on the pathline images below.

The particle that hits the flat surface will have a much higher impact because the state of the particle motion is not changed. Swirling flow is caught in the grooves and slows down the velocity of the particles. The particles hit the surface at a much slower velocity and lesser impact on the grooved surface. The impact speed of particles will be reduced when they go through the turbulence layer on the grooved surface. The turbulent layer reduces the momentum of the particles that hit the surface and decreases the number of particles impinging on the surface. As a result, the erosion damage on the surface of the substrate is reduced.

We observe that fatigue cracks mostly initiate at the sites of stress concentrations. Once a crack initiates, we will also have to consider the stress concentration of the crack. This crack will only propagate when the energy needed for it is sufficient enough to overcome the resistance of the material. Once the threshold toughness for crack initiation is exceeded, the energy required for crack extension is so low that it can be provided by the release of stored elastic energy in the system from the DPM Particle collisions. This is when we observe the

highly preferential material and mass loss over the surface geometry, visible in the erosion contour images below.

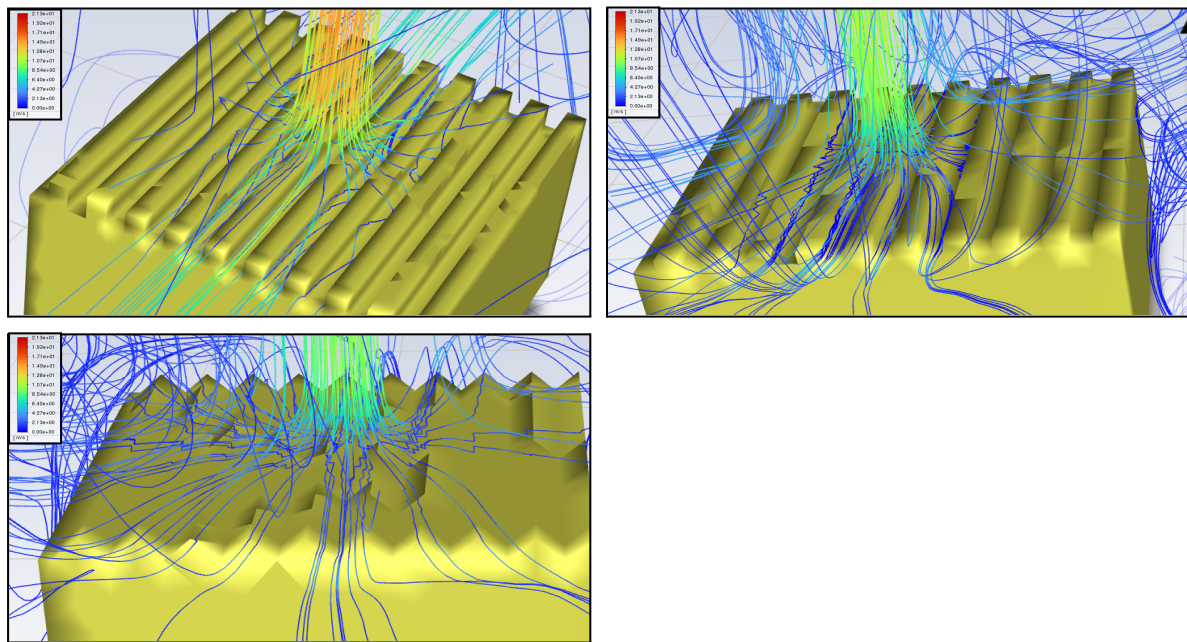


Fig. 12 Velocity Coloured Pathline Figures of the DPM Particles striking the surface and depicting rebounding within the surface textures at different trajectories for different samples. (Marked in Red)

- (Top Left) 0.3mm Depth Square Section Microchannels
- (Top Right) 0.6mm Depth Square Section Microchannels
- (Bottom Left) 0.5mm Depth V Section Microchannels

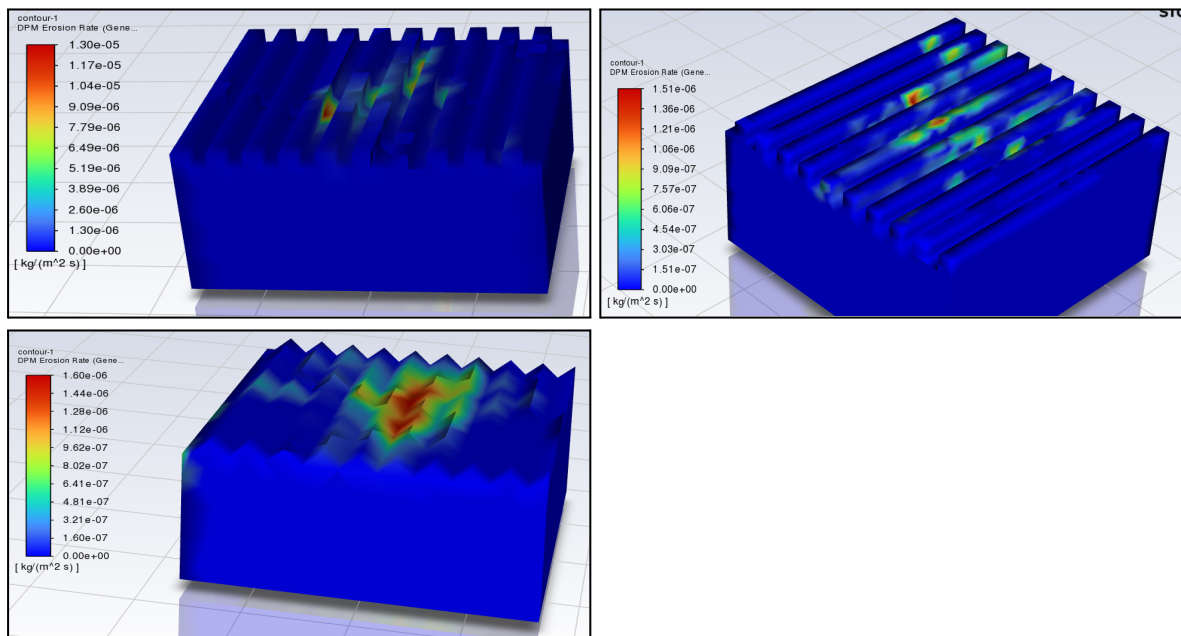


Fig. 13 Generic Erosion Rates coloured contour figures of the textured substrates correlating stress concentration and material loss.

- (Top Left) 0.5mm Depth Square Section Microchannels
- (Top Right) 0.6mm Depth Square Section Microchannels
- (Bottom Left) 0.5mm Depth V Section Microchannels

4. Conclusions

Our work began with an extensive literature review about Surface Degradation and Damage, material loss due to several tribological factors, Surfaces Textures and their advantages. With this project we wanted to understand the effect of various texture parameters such as Variations in Texture Depth, Cross Section Shape and Pattern types on the overall erosion rate of the substrate, by simulating and analyzing them using Computational Fluid Dynamics (CFD). The ANSYS Workbench and Fluent 2022 R1 Software was used for all our simulations. Various substrates of different surface textures were modeled on SpaceClaim 2022 R1 and then meshed. The simulation was set up, using the Realizable K- ϵ Model for Turbulence Modeling and Discrete Phase Model (DPM) for modeling erosion wear. Submerged Slurry Erosion was experimentally performed to validate the simulation setup. Stainless Steel SS316L was polished, ultrasonicated and then subject to Submerged Slurry Erosion and its values were compared with the simulation values to validate the chosen erosion model. The time averaged erosion rates for all the other textured substrates were then calculated and compared across different parameters.

We were able to obtain optimum values for the three parameters under study, with a 0.6mm texture depth, V-Shape Cross Section and Microchannels showing the lowest erosion rates respectively. We account this behavior to the different erosion mechanisms taking place on the surface of the substrate and within the textures, with flow disruption, stress concentration and increased hardness all very important factors in deciding the overall erosion rates.

This project shows the potential to develop a Global Optimum Texture which would theoretically show the least material loss and erosion rates under similar flow conditions. The future scope of this project as an extension definitely involves exploring the manufacturing process required for creation of surface textures to understand if they also contribute to the overall erosion mechanisms, understanding how to scale up the processing for industrial applications, optimizing other surface parameters such as roughness, spacing and width. This work has been done keeping applications within the Maritime Industry in mind however the erosion mechanisms can be modeled similarly for almost any other applications, with the aim of minimizing material degradation due to tribological factors.

5. References

- [1] D. W. Bechert, M. Bruise, W. Hage. “Experiments with three-dimensional ripples as an idealized model of shark skin”, Experiments in Fluids, 2000.
- [2] Radha, Lim, Saifullah, Kulkarni. “Metal hierarchical patterning by direct nanoimprint lithography”. Scientific Reports, 2013.
- [3] Sinmazcelik, Fidan, Urgun. “Effects of 3D printed surface texture on erosion wear”, Tribology International, 2019.
- [4] Arumugaprabu, Ko, Kumaran, Kurniawan, Uthayakumar. “A brief review on importance of surface texturing in materials to improve the tribological performance”. Rev.Advanced Material Science, 2018.
- [5] Jung, Yang, Jung, Kim. “Anti-erosion mechanism of a grooved surface against impact of particle-laden flow”. Wear, 2018.
- [6] Han, Yin, Jiang, Niu, Ren. “Erosion-Resistant surfaces inspired by Tamarisk”. Journal of Bionic Engineering, 2013.
- [7] Zhao, Tang, Liu, Zhang. “Finite element analysis of anti-erosion characteristics of material with patterned surface impacted by particles”. Powder Technology, 2018.
- [8] R.B. Nair, H.S. Arora, S. Mukherjee, S. Singh, H. Singh, H.S. Grewal. “Exceptionally High Cavitation Erosion and Corrosion Resistance of a High Entropy Alloy”. Ultrasonics Sonochemistry, 2017,
- [9] Xu, Zhang, Zhou, Gao, Wang, Wang, Huang. “Flow accelerated corrosion and erosion-corrosion behavior of marine carbon steel in natural seawater”. Materials Degradation, 2021.
- [10] Sohn, Yang, Lee, Park. “Sensing solutions for assessing and monitoring of nuclear power plants (NPPs)”. Sensor Technologies for Civil Infrastructures.
- [11] Ramesh Padavala.”Failure Mechanisms in impact erosion of ductile materials”. Graduate Theses, Dissertations and Problem Reports. 2004.
- [12] Batchelor, Lam and Chandrasekaran. “Materials Degradation and its control by surface engineering”. 2nd Edition, Imperial College Press 2002.

- [13] Lopez, Nicholls, Stickland, dempster. "CFD Study of Jet Impingement Test erosion using Ansys Fluent and Open FOAM". Computer Physics Communication, 2015.
- [14] Khanouki, Zahedi, Shirazi and McLaury. "Erosion modeling in high concentration slurry flows". Proceedings of the ASME 2017 Fluids Engineering Division Summer Meeting, August 2017.
- [15] Mansoue, Badr, Araoye and Toor. "Computational Analysis of Water Submerged Jet Erosion". Energies, May 2021.
- [16] Arabnejad, Mansouri, Shirazi and McLaury. "Abrasion erosion modeling in particulate flow". Elsevier Wear, January 2017.
- [17] Karimi, Mansouri, Shirazi and McLaury. "Experimental investigation on the influence of particle size in a submerged slurry jet on erosion rates and patterns". Proceedings of the ASME 2017 Fluids Engineering Division Summer Meeting, August 2017.
- [18] Perez. "Enhancing tribological properties of metallic sliding surfaces through micro multi texturing techniques". Graduate Thesis, University of Calgary, July 2019.
- [19] Javaheri, porter, Kuokkala. "Slurry erosion of steel - Review of tests, mechanisms and materials". Elsevier Wear, July 2017.
- [20] Divakar, Agarwal and Singh. "Effect of the material surface hardness on the erosion of AISI316". Elsevier Wear, July 2005.
- [21] ANSYS Inc. "ANSYS Fluent Theory Guide". Release 15.0 November 2013.
- [22] Pandya. Development of computational fluid dynamics (CFD) based erosion models for oil and gas industry applications". Doctoral Thesis, The University of Texas At Arlington, December 2013.
- [23] Marrah. "Simulating of Erosion Modeling using ANSYS Fluid Dynamics". Masters Thesis, Faculty of Engineering and Applied Science, Memorial University of Newfoundland, May 2019.
- [24] Bajracharya, Shrestha, Timilsina. "Solid Particle Erosion Models and their Application to Predict Wear in Pelton Turbine Injector". Journal of the Institute of Engineering, October 2019.

- [25] Singh, Kumar et al. “CFD modeling of erosion wear in pipe bend for the flow of bottom ash suspension”. Particulate Science and Technology, October 2017.
- [26] Grewal, Singh and Yoon. “Interplay between erodent concentration and impingement angle for erosion in dilute water-sand flows”. Wear Elsevier, February 2015.
- [27] Morris, Shahmohamadi, Rahmani and Rahnejat. “A CFD Study Comparing Surface Texture Features on Stationary and Entraining Surfaces”. 42nd Leeds-Lyon Symposium on tribology, September 2015.
- [28] Na, Kim and jeon. “Analysis of Erosion Minimization for a Slurry Pump Using Discrete Phase Model Simulations”. Applied Sciences, February 2022.